

FLNeRF: 3D Facial Landmarks Estimation in Neural Radiance Fields

Hao Zhang^{*1} Tianyuan Dai^{*1} Yu-Wing Tai^{1,2} Chi-Keung Tang¹

¹The Hong Kong University of Science and Technology

²Kuaishou Technology

{hzhangcc, tdaiaa}@connect.ust.hk, yuwing@gmail.com, cktang@cse.ust.hk

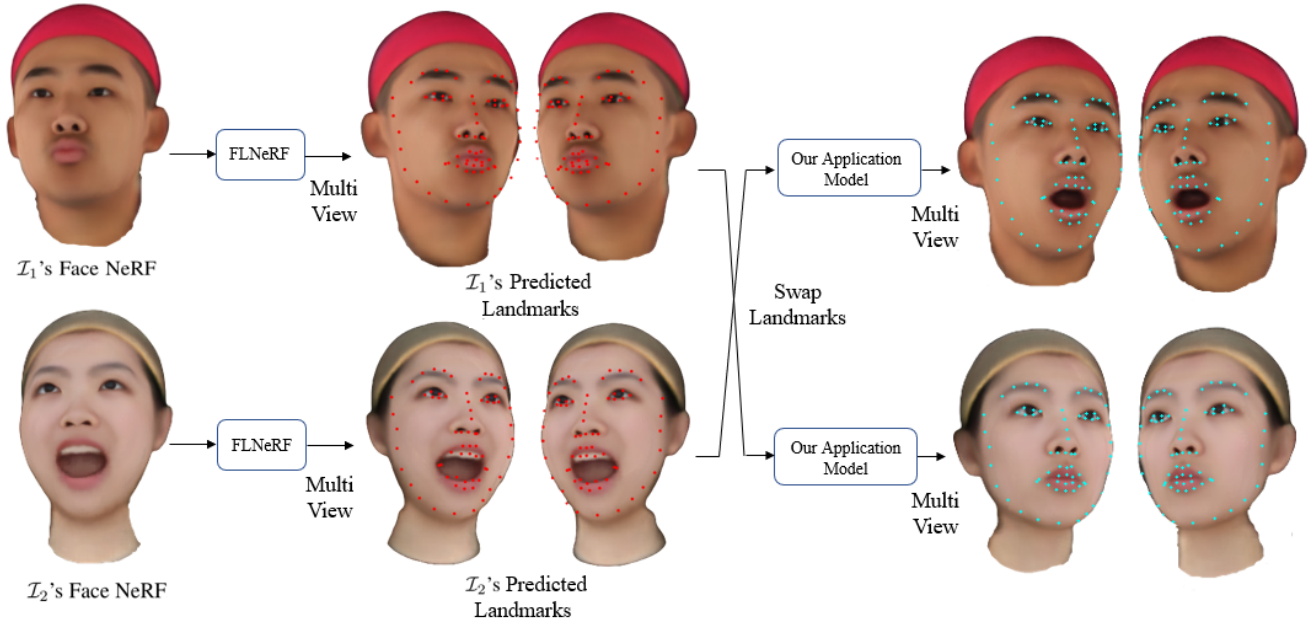


Figure 1. **Accurate 3D landmarks on face NeRF.** FLNeRF directly operates on dynamic NeRF, so that an animator can easily edit, control and even transfer emotion from another face NeRF. With precise landmarks on facial features (eye brows, nostrils, mouth), exaggerated facial expressions with wide grinning, mouth wide open, cheek blowing can be readily achieved.

Abstract

This paper presents the first significant work on directly predicting 3D face landmarks on neural radiance fields (NeRFs), without using intermediate representations such as 2D images, depth maps, or point clouds. Our 3D coarse-to-fine Face Landmarks NeRF (FLNeRF) model efficiently samples from the NeRF on the whole face with individual facial features for accurate landmarks. To mitigate the limited number of facial expressions in the available data, local and non-linear NeRF warp is applied at facial features in fine scale to simulate large emotions range, including exaggerated facial expressions (e.g., cheek blowing, wide opening mouth, eye blinking), for training FLNeRF. With such expression augmentation, our model can predict 3D landmarks not limited to the 20 discrete expressions given in the data. Robust 3D NeRF facial land-

marks contribute to many downstream tasks. As an example, we modify MoFaNeRF to enable high-quality face editing and swapping using face landmarks on NeRF, allowing more direct control and wider range of complex expressions. Experiments show that the improved model using landmarks achieves comparable to better results. Github link: <https://github.com/ZHANG1023/FLNeRF>.

1. Introduction

Neural Radiance Field (NeRF) is a game-changing approach to 3D scene representation model for novel view synthesis, which represents a static 3D scene by a fully-connected neural network [38]. The network, directly trained on 2D images, is optimized to approximate a continuous scene representation function which maps 3D scene coordinates and 2D view direction to a view-dependent color and a density value. The implicit 5D continuous scene representation allows NeRF to represent more complex and

^{*}Equal Contribution

subtle real-world scenes, overcoming reliance of explicit 3D data, such as 3D voxels and point clouds, where custom capture, sensor noise, and discrete representations are long standing issues. Further studies [8, 21, 25, 27, 29, 33, 34, 39, 51–53, 61, 63, 67, 72, 77, 81, 84] have been done to improve the performance, efficiency and generalization of NeRF, with its variants quickly and widely adopted in dynamic scene reconstruction [15, 32, 46, 49, 76], novel scene composition [24, 30, 36, 40, 42, 45, 79, 82], articulated 3D shape reconstruction [7, 28, 43, 48, 55, 73, 78, 80, 86, 87] and various computer vision tasks, including *face NeRFs* [2, 14, 19, 26, 44, 64], this paper’s focus, which require the pertinent models to represent both subtle expressions and large emotion ranges, unlike previous models on 3D mesh, point cloud and other discrete voxel-based methods despite their successes in large-scale 3D reconstruction and synthesis.

While NeRF-related works have been proposed for face reconstruction, single-image face NeRF estimation, and face novel view synthesis, to our knowledge, no significant work has been done to predict 3D face landmarks on NeRFs. 3D face landmarks are useful in downstream tasks, e.g., face recognition, identification, and face alignment. Our work, dubbed as **FLNeRF**, is the first work to accurately estimate 3D face landmarks directly on NeRFs.

FLNeRF contributes a coarse-to-fine framework to predict 3D face landmarks directly on NeRFs, where keypoints are identified from the entire face region (coarse), followed by detailed keypoints on facial features such as eyebrows, cheekbones, and lips (fine). Such coarse-to-fine framework is memory and run-time efficient. Our framework is directly trained on FaceScape [88] where each identity contains 20 discrete expressions. To cover expressions beyond these 20, such as those showing half-open mouth, closed eyes, and even smiling fish face, we propose to augment more facial expressions in FaceScape, by applying local and non-linear warp on the relevant facial features with careful manual labeling of keypoints. Consequently, the augmented FaceScape contains 110 expressions, including subtle as well as exaggerated expressions. This expressive facial data set will also be available.

We believe that 3D facial landmarks have the potential of representing substantial information of facial shape and expression, which are two of three sets of parameters in 3DMM [68]. A recent work MoFaNeRF [93] embeds texture, shape, and expression into a space and render novel views of human faces. By replacing their shape and expressions codes with our facial landmarks, we show how direct control using landmarks can achieve comparable or even better results on face editing and swapping.

In summary, our main contributions are three-fold:

- We propose FLNeRF, a coarse-to-fine 3D face landmark predictor on NeRFs, as the first significant model for 3D face landmark estimation directly on NeRF without any intermediate representations. Leveraging NeRF’s inherent continuity, our model gives accurate

approximation of 68 face landmarks.

- We enrich FaceScape [88] from 20 to 110 discrete expressions with a data augmentation method based on non-linear NeRF warp. By training FLNeRF on the expanded data set, face landmarks on a wider range of expressions can be accurately estimated.
- We demonstrate impressive applications by benefiting MoFaNeRF [93], replacing shape and expression code with our accurate 3D face landmarks directly estimated from NeRFs. Given accurate 3D landmarks, our improved MoFaNeRF performs multiple high-quality downstream tasks of 3D face landmark prediction, such as face editing and face swapping (Figure 1).

2. Related Work

2D Face Landmarks Prediction Active Shape Models (ASM) [1, 10, 11] and Active Appearance Models (AAM) [9, 54] are classic methods in 2D face landmarks prediction and alignment. Today CNN-based methods have become mainstream which typically fall into two categories: heatmap regression models, and coordinate regression models. Heatmap-based models [65, 71, 75, 89] generate probability maps for each landmark location. However, face landmarks are not independent sparse points, but have inherent interdependency. Heatmap-based methods are prone to occlusion and appearance variations due to lack of structural information of face landmarks. In contrast to heatmap regression models, directly learning landmarks coordinates have the natural potential to encompass structural information [31, 69]. Majority of coordinate-based methods [37, 60, 66, 70, 90] progressively migrate predictions toward ground truth landmark points on 2D image. Nevertheless, even though coordinate regression models are infused with weak structure knowledge, these methods still lack knowledge about 3D structure of face landmarks by only making use of 2D images without 3D information.

3D Face Landmarks Prediction Structure information is more substantial in 3D space. 3D Morphable Model (3DMM) [4] is among the earliest methods in representing 3D face which decouples 3D facial attributes into shape and appearance. Due to its strong 3D prior, 3DMM is generally used as an intermediate to guide learning of face models. Before NeRFs, traditional 3D scene representation methods include voxel, mesh, and point cloud.

Voxel-based methods [56, 57, 83] reconstruct face by producing deep features and regressing coordinates of face keypoints. Most of them also adopt the coarse-to-fine framework. Compared to 2D methods, voxel-based models consider more structure information, thus are more robust against occlusion and large pose and expression variances. However, voxel-based methods are memory expensive and take long time for rendering face images. Mesh-based methods [17, 22, 41, 59, 74, 91] localize 3D face landmarks by reconstructing 3D face mesh. Compared to vox-

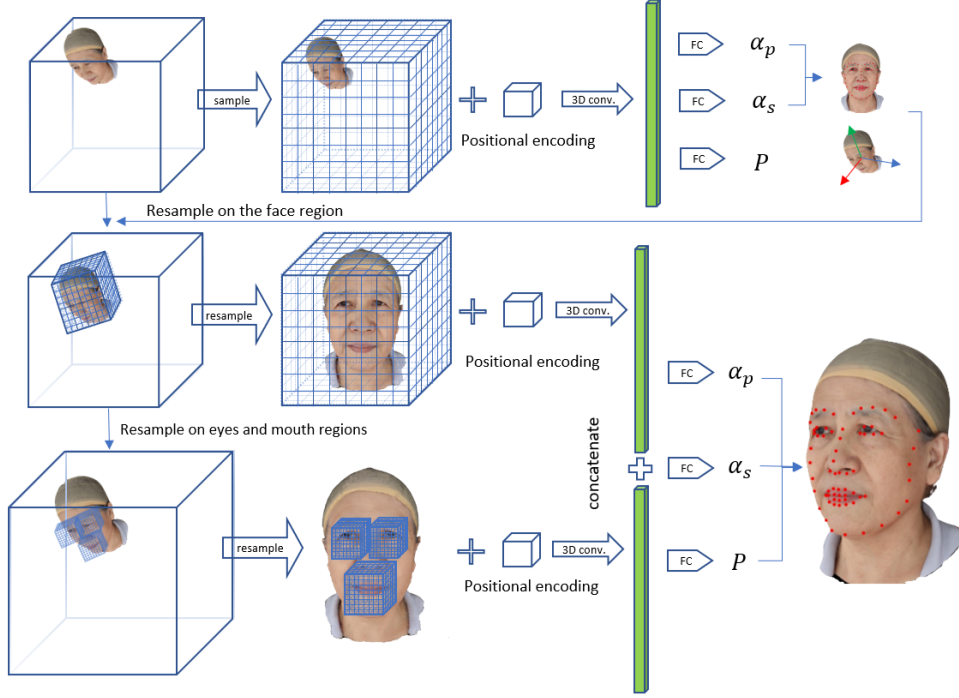


Figure 2. **FLNeRF pipeline of our 3D facial landmarks detection.** We choose 4 representative regions i.e., eyes, mouth and the whole face to detect facial landmarks. In each region, 4 channel volumes are sampled from the NeRF. Together with the 3D position encoding, these 7 channel volumes will be encoded as a 1D vector by 3D VolResNet or VGG backbone. Four separate 1D vectors received from the 4 coarse-to-fine scales (i.e., the whole face, left and right eyes including eyebrows, and lips including philtrum and cheekbone regions) are concatenated and decoded to 3DMM parameters and pose (given by the transform matrix) using MLPs.

els, mesh-based methods require less for storing polygons. Point cloud-based methods [3, 12, 16, 23, 47, 62] either directly learn from point cloud, or reconstruct point cloud from images. Despite their successes, point cloud-based methods require high-quality and thus often need expensive custom capture. By contrast, RGB-D images can be obtained by low-cost sensors while still containing 3D information. Methods using RGB-D images as training data [13, 50, 85, 92] usually first construct voxel or mesh and then make prediction based on such representation.

Traditional 3D face landmarks localization methods have limited range of expression and pose variations, due to the discrete representation of voxels, meshes, and point clouds. While low-resolution processing leads to severe information loss, high-resolution processing induces large memory footprint and long training and rendering time. Since an expressive face contains important subtle features which can easily get lost using such discrete representations, a continuous representation is preferred.

Face NeRFs Since NeRF represents 3D face continuously as solid (i.e., unlike point cloud crust surface), and only requires multiview RGB images with camera poses, applying NeRF on face-related tasks have recently intrigued research effort. In [20], portrait NeRF is constructed from a single RGB headshot, but requires custom capture, or a light-stage dataset for meta-learning. In [19], the authors combined a

scene representation network with a low-dimensional morphable model, while [2] utilizes a deformation field and uses a 3D morphable face model (3DMM) as a deformation prior. In [44] a NeRF-style volume renderer is used to generate high fidelity face images. In face editing and novel view synthesis, training NeRF generators [14, 26, 64] reveals promising prospects for the inherently continuous 3D representation of the volume space, with drastic reduction of demanding memory and computational requirements of voxel-based methods. FENeRF [64] utilizes monocular images with paired semantic masks to produce view-consistent and locally-editable portraits, while the NeRF generator and GAN training are still costly. To tackle this, [14] confines points sampling and radiance learning on 2D manifolds embodied as a set of implicit surfaces. HeadNeRF [26] further accelerates the rendering process by integrating 2D neural rendering into the rendering procedure of NeRF. MoFaNeRF [93] encodes appearance, shape, and expression into a latent vector space and directly synthesizes photo-realistic face. Continuous face morphing can be achieved by interpolating the three codes. We modify MoFaNeRF in Sec. 4 to support high-quality face editing and face swapping by directly manipulating face landmarks predicted on NeRF which clearly demonstrates the advantages of 3D landmarks control.

3. 3D Face NeRF Landmarks Detection

Figure 2 shows the pipeline of FLNeRF which is a multi-scale coarse-to-fine 3D face landmarks predictor on NeRF.

Our coarse model takes a face NeRF as input, and produces rough estimation of the 3DMM parameters, location and orientation of the input face by 3D convolution of the sampled face NeRF with position encoding. Unlike SynergyNet [74] which crops faces in 2D images, our coarse model can localize the pertinent 3D head in the NeRF space. Based on the estimated coarse landmarks, our fine model resamples from four regions: whole *face*, the left and right *eyes* including eyebrows, and *mouth* including lips, philtrum and cheekbone regions. In our coarse-to-fine implementation, the resolution of the resampled 3D volumes (coarse or fine) are respectively 64^3 .

The resampled volumes are then used to estimate more accurate 3DMM parameters with position encoding in Sec. 3.1. After describing how to benefit from the underlying continuous NeRF representation in sampling in Sec. 3.2, we will explain our coarse model in Sec. 3.3 and fine model in Sec. 3.4. Since there are only 20 discrete expressions in FaceScape [88] with fixed head location and orientation, more diverse expressions and head poses are not covered in the dataset. To alleviate this limitation, we apply data augmentation to enrich our dataset to 110 expressions with different head poses per person, allowing our model to accurately locate and predict landmarks for faces with more complex expressions. We will describe our coarse data augmentation and fine expressions augmentation in Sec. 3.5.

3.1. 3DMM

We follow SynergyNet [74] to estimate parameters of 3D Morphable Model (3DMM) to approximate face geometry. The reconstructed face mesh $S_f \in \mathbb{R}^{3 \times N_v}$ with N_v 3D vertices can be represented by Eq. (1).

$$S_f = \text{Mat}(M + U_s \alpha_s + U_e \alpha_e) \quad (1)$$

where $M \in \mathbb{R}^{3N_v}$ is the mean face with N_v 3D vertices, $U_s \in \mathbb{R}^{3N_v \times 40}$ and $U_e \in \mathbb{R}^{3N_v \times 10}$ is the basis for shape and expression variations manifold, $\alpha_s \in \mathbb{R}^{40}$ and $\alpha_e \in \mathbb{R}^{10}$ are the corresponding basis coefficients.

To align S_f with an input face NeRF, a transform matrix $P \in \mathbb{R}^{3 \times 4}$ is predicted. New aligned face mesh can be written as:

$$S_v = P \begin{bmatrix} S_f \\ 1 \end{bmatrix} \quad (2)$$

After reconstructing face mesh from 3DMM, 3D landmarks $L \in \mathbb{R}^{N \times 3}$ can be extracted from predefined landmark indices. After that, the 3DMM mesh is neither used in training and testing.

3.2. NeRF Sampling

NeRF is a continuous representation underlying a 3D scene. So far, most feature extractors are applied in dis-

crete spaces such as voxel, mesh and point cloud, which inevitably induces information loss. In order to maximize the benefit of the continuous representation, we adopt a coarse-to-fine sampling strategy. Specifically, given a NeRF containing a human head, uniform coarse sampling will first be performed in the whole region of the NeRF with respect to the radiance and density channels to generate feature volumes (RGB is used to represent radiance). Because FaceScape [88] only contains the images of frontal head, we assume the viewing direction is looking at the frontal face when we sample the NeRF, which helps to make the radiance sampled on the face surface more accurate. We only utilize the radiance and density queried at given points of the NeRF, thus our model is applicable to most NeRF representations. To discard noisy samples, voxels with density smaller than a threshold (set to 20 by experiments) will be set to 0 in all channels (RGB and density), and voxel with density larger than the threshold will have the value one in density channel with RGB channels remaining the same. In the fine sampling, given the predicted coarse landmarks, orientation and translation of the head by the coarse model, the sampling regions of the whole face, eyes, and mouth are cubic boxes centered at the mean points of the landmarks belonging to corresponding regions with a suitable size proportional to the scale of the head. These cubic sampling boxes are aligned to the same rotation of the head. The same noise discarding strategy is used here.

3.3. Coarse Model

Inspired by the CoordConv [35], to enhance ability of 3D CNNs to represent spatial information, we add position encoding channels to each feature volume. Instead of directly using the Cartesian coordinates, a higher dimensional vector encoded from x, y, z normalized to $[0, 1]$ are used as position encoding. The mapping function from x, y, z to higher dimensional space is modified from that in [38] which includes the original Cartesian coordinates:

$$\gamma(p) = (p, \sin(2^0 \pi p), \cos(2^0 \pi p), \dots, \sin(2^{L-1} \pi p), \cos(2^{L-1} \pi p)). \quad (3)$$

We set $L = 4$ and $\gamma(\cdot)$ is applied to individual coordinate.

We adopt the VoxResNet [6] and 3D convolution version of VGG [58] as our backbone to encode the pertinent feature volumes into a 1D long vector. Similar to SynergyNet [74], three separate fully-connected layers are used as decoder to predict the transform matrix and 3DMM parameters. The transform matrix contains the head location and orientation. The 68 landmarks can be extracted from the pre-defined landmark indices of the 3DMM. The loss we used is the Wing loss [18]:

$$\text{wing}(x) = \begin{cases} \omega \ln(1 + |x' - x|/\epsilon) & \text{if } |x' - x| < \omega \\ |x' - x| - C & \text{otherwise} \end{cases} \quad (4)$$

where we set $\omega = 10$ and $\epsilon = 2$. The $x' \in \mathbb{R}^{204 \times 1}$ is

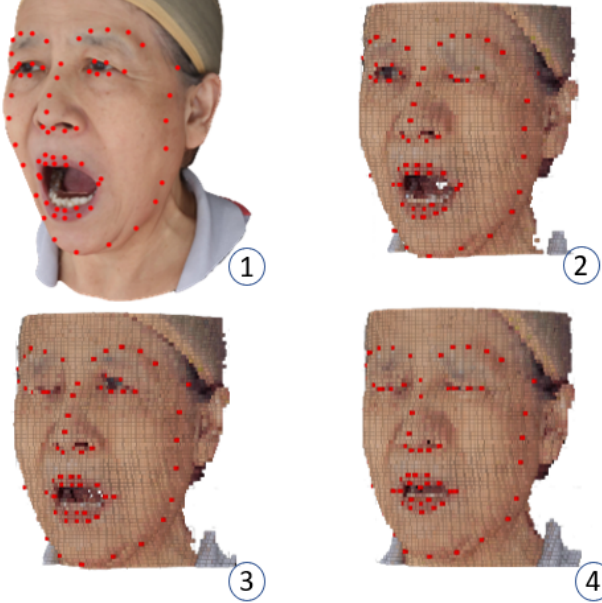


Figure 3. **Expression augmentation.** Subfigure 1 is the original stretch mouth NeRF with facial landmarks. Others are the feature volumes sampled non-uniformly from this NeRF using 3D TPS with the target landmarks.

reshaped from the predicted landmarks $\in \mathbb{R}^{68 \times 3}$. The $x \in \mathbb{R}^{204 \times 1}$ is reshaped from GT landmarks $\in \mathbb{R}^{68 \times 3}$.

3.4. Fine Model

With the location, orientation and the coarse landmarks of the face given by the coarse model, a bounding box aligned with the head can be determined. Usually, the eyes and mouth have more expressive details. The bounding box of the eyes and mouth can also be determined, according to the coarse landmarks. Due to the low sampling resolution used in the coarse model and the inaccuracy of the coarse model prediction, the bounding boxes will be made slightly larger to include all necessary facial features and their proximate regions. The same sampling method and position encoding as the coarse model will be performed on these bounding boxes. Similar to the coarse model, VoxResNet or 3D convolution version of VGG is used as the backbone to encode these four feature volumes as four 1D long vectors. These 1D long vector containing expressive information on eyes, mouth and the whole face are concatenated to predict the 3DMM parameters and a transform matrix. Finally, fine 3D landmarks can be extracted from these 3DMM parameters. The loss function is same as that in the coarse model.

3.5. Data and Expression Augmentation

3.5.1 Data augmentation for coarse model

FaceScape contains faces situated at the origin and facing forward. Taking into account NeRF implementations with different scales or coordinate systems, to boost the generality of our FLNeRF to support 3D landmarks prediction on a wide variety of input NeRF containing a head, we augment

the data set with various face locations, orientations and scales. Instead of training a new NeRF which is more time-consuming, we perform data augmentation during sampling these NeRFs into feature volumes $\in \mathbb{R}^{4 \times N \times N \times N}$ and assume the meaningful region of NeRF is $\in [0, 1]^3$, which can be easily normalized as such otherwise. Each sampled point $S \in [0, 1]^3$ will be transformed by a matrix $\tau[\mathbf{R}t]$ to a new position, where $\mathbf{R} \in SO(3)$, $\tau \in [2, 3]$ and $t \in [-1, 1]^3$. New augmented feature volumes are generated by sampling NeRF at new sampling position. This operation is equivalent to scale, translate and rotate the head in the feature volumes. Although the sampled points may lie outside the captured NeRF, the density of these points is usually less than the threshold set ahead. Even some density exceeds the threshold, they are just some random noise points in the feature volumes that will be ignored by our FLNeRF.

3.5.2 Expression augmentation for fine model

Figure 3 illustrates our data augmentation to include more expressive facial features for training. In summary, a total of 90 expression volumes from FaceScape [88] are sampled non-uniformly from the given 20 expression NeRFs using 3D thin plate spline (3D TPS) [5]. Note that the variation of the 20 discrete expressions in the FaceScape [88] is insufficient for training 3D landmarks detector on the NeRF to cover wide range of facial emotions. Given a original N 3D landmarks $\mathbf{L} \in \mathbb{R}^{N \times 3}$ and the target N 3D landmarks $\mathbf{L}' \in \mathbb{R}^{N \times 3}$, we can construct Eq. (5) to warp $\mathbf{x} \in \mathbb{R}^3$ to $\mathbf{x}' \in \mathbb{R}^3$. Let $[l_1, l_2, \dots, l_{N-1}, l_N]^T = \mathbf{L}$ and $[l'_1, l'_2, \dots, l'_{N-1}, l'_N]^T = \mathbf{L}'$:

$$\mathbf{x}' = f(\mathbf{x}) = \mathbf{A}_0 + \mathbf{A}_1 \mathbf{x} + \sum_{i=1}^N \omega_i U(\|\mathbf{l}_i - \mathbf{x}\|) \quad (5)$$

where

$$\mathbf{A}_0 = \begin{bmatrix} a_x \\ a_y \\ a_z \end{bmatrix} \quad \mathbf{A}_1 = \begin{bmatrix} a_{xx} & a_{xy} & a_{xz} \\ a_{yx} & a_{yy} & a_{yz} \\ a_{zx} & a_{zy} & a_{zz} \end{bmatrix} \quad \omega_i = \begin{bmatrix} \omega_{ix} \\ \omega_{iy} \\ \omega_{iz} \end{bmatrix} \quad (6)$$

$\mathbf{A}_0 + \mathbf{A}_1 \vec{x}$ is the best linear transformation mapping \mathbf{L} to \mathbf{L}' . $U(\|\mathbf{x}_i - \mathbf{x}\|)$ measures the distance from \mathbf{x} to control points \mathbf{L} . We use $U(r) = r \log(r^2)$ as the radial basis kernel and $\|\cdot\|$ denotes L_2 norm. These coefficients \mathbf{A}_0 , \mathbf{A}_1 and ω_i can be found by solving a linear system (supp mtrl).

In summary, a warped feature volume can be sampled non-uniformly from a NeRF by 3D TPS warp specified by the original and target landmarks. We use a linear combination of original expression landmarks, and manually specify expression landmarks to generate 90 more expression landmarks. For each person in the FaceScape data set, a total of 110 expressions are available for training.

4. Applications

Face editing using 2D/3D landmarks as input has been widely adopted by professional animators and amateurs

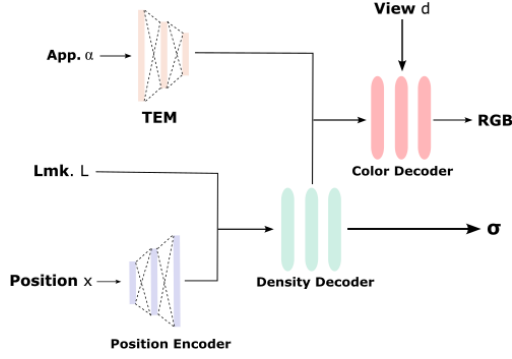


Figure 4. Architecture of **Modified MoFaNeRF model (2-code model)**, where we replace their shape and expression codes by our landmarks with position encoding. Appearance code which encodes the face texture remains the same. TEM is texture encoding module in [93].

alike due to their direct and easy control to achieve expressive facial emotions. Despite NeRF’s compelling representation power and efficiency, there has been no representative work on 3D face NeRF landmarks detection that enables NeRF landmark-based applications (such as face swapping and expression editing) while producing realistic 3D results on par with ours. In this section, we will show how the landmarks estimated by FLNeRF can immediately benefit the state-of-the-art MoFaNeRF [93].

While MoFaNeRF generates SOTA results, we believe the range of expressive emotions is limited by its shape and expression code. A detailed analysis is given in the appendix on their disentanglement of shape and expression in [93]. 3D NeRF facial landmarks on the other hand provides *explicit* controls on facial expressions including fine and subtle details from exaggerated facial emotions. To directly benefit MoFaNeRF, we simply replace their shape and expression code with our 3D face landmarks location, which allow us to directly control NeRF’s facial features and thus produce impressive results on morphable faces, face swapping and face editing, alleviating the two limitations of MoFaNeRF (appendix). The ablation studies in this section validate that our 3D facial landmarks on NeRFs have stronger representation power than combination of shape and expression codes.

4.1. Model Architecture

Our modified MoFaNeRF model architecture is shown in Fig. 4, where we remove shape code, expression code, and ISM in the original MoFaNeRF model (reviewed in the appendix). This is because by [93]’s design, expression code is learnable, while shape code remains the same among all expressions of the same identity. However, face shape including location of mouth and eyebrows may also change during expression changes (e.g., brow raises, brow lowers, mouth twists to left or right, mouth stretches, jaw moves to left or right, etc). The combination of a static shape code with a learnable expression code may thus conflict with each other.



Figure 5. **Demonstration of face swapping by swapping landmarks.** The first row consists of rendered images from two different views by respectively feeding \mathcal{I}_1 ’s and \mathcal{I}_2 ’s texture map with ground truth landmarks to generate the pertinent NeRFs using our modified MoFaNeRF. The second row shows images generated by respectively feeding to the network \mathcal{I}_1 ’s landmarks with \mathcal{I}_2 ’s texture map, and \mathcal{I}_2 ’s landmarks with \mathcal{I}_1 ’s texture map.

Instead, we directly concatenate 3D face landmarks to the encoded space position. The concatenated vector is fed into the density decoder. By doing so, our model takes in 3D space location, view direction, texture code, and 3D face landmarks as inputs to generate a face NeRF. Given texture map, we can render a face image with any given expression from any view points by manipulating the face landmarks. We adopt the same training configurations as [93].

Since our FLNeRF, which is trained on expanded data set with 110 expressions, can produce accurate 3D face landmark locations, and that our modified MoFaNeRF operates on landmarks directly, we can perform downstream tasks employing our face landmarks prediction on NeRF, i.e., face editing and face swapping.

4.2. Face Swapping

We can swap the expressions of two identities by swapping their 3D landmarks. Two identities \mathcal{I}_1 and \mathcal{I}_2 may have different ways to perform the same expression. Feeding \mathcal{I}_2 ’s landmarks on a given facial expression with \mathcal{I}_1 ’s texture map to our modified MoFaNeRF enables \mathcal{I}_1 to perform the corresponding expression in \mathcal{I}_2 ’s way, the essence of face swapping. We show our modified MoFaNeRF can perform face swapping in Fig. 5, where the man takes on the woman’s landmarks to produce the corresponding expression faithful to the woman’s, and vice versa.

By connecting the modified MoFaNeRF at the end of our FLNeRF, so as to perform downstream face swapping task after obtaining accurate prediction of 3D face landmarks, Fig. 1 shows that given two face NeRFs and their respective face landmarks, we can swap their expressions by simply swapping their face landmarks on NeRF. In detail, given the landmarks and textures of \mathcal{I}_1 and \mathcal{I}_2 , we obtain their respective face NeRFs by our modified MoFaNeRF, where we

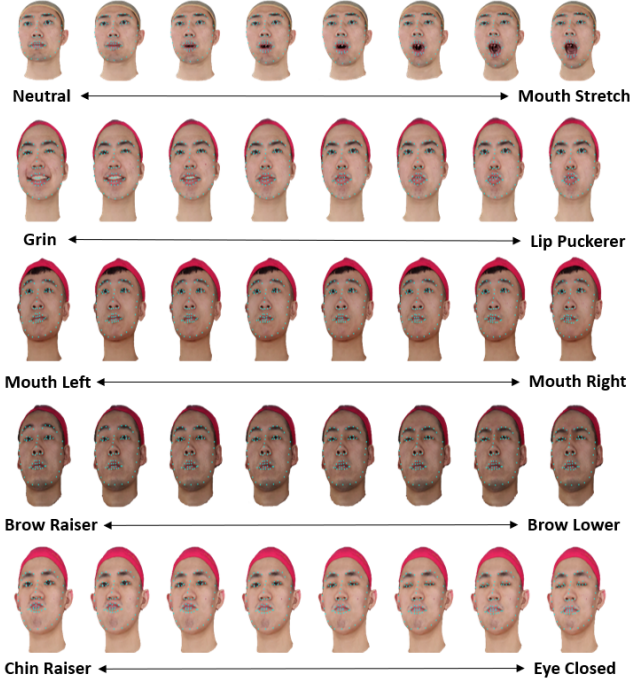


Figure 6. Demonstration of **face editing** via direct landmark control. For each row, images are rendered by interpolating landmarks of the left most expression and the right most expression.

apply FLNeRF to predict landmarks on these input two face NeRFs. The predicted landmarks of \mathcal{I}_1 are fed to the modified MoFaNeRF with \mathcal{I}_2 's texture map, while predicted landmarks of \mathcal{I}_2 are fed to the modified MoFaNeRF with \mathcal{I}_1 's texture map. In doing so, our modified MoFaNeRF can synthesize swapped face images from any view direction.

4.3. Face Editing

We can produce an identity's face with any expression given the corresponding landmarks and texture. Fig. 6 shows that our model can morph face by directly manipulating landmarks, where images on each row are rendered from NeRFs synthesized by linearly interpolating between the two corresponding NeRFs with landmarks of the left-most expression and landmarks of the rightmost expression. Fig. 6 clearly demonstrates that our model can produce complex expressions even not included in our dataset. For example, middle images in the fifth row demonstrate our model's ability to represent a face with simultaneous chin raising and eye closing. Fig. 6 also shows that we can independently control eyes, eyebrows, mouth, and even some subtle facial muscles, with better disentanglement ability over MoFaNeRF [93] using shape and expression code.

We connect our modified MoFaNeRF at the end of FLNeRF, so as to perform downstream face editing after obtaining accurate prediction of 3D face landmarks. Fig. 7 shows that we can transfer one person's expression to another. In detail, we first obtain a face NeRF with the desired expression by feeding the corresponding landmarks into the modified MoFaNeRF. Then we apply our FLNeRF on the

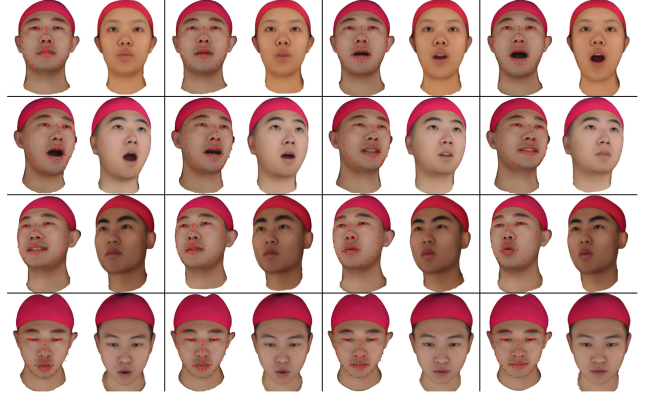


Figure 7. Demonstration of **expression transfer** by connecting the modified MoFaNeRF to FLNeRF as a downstream task. For each pair of images, the left face is the driver face, where landmarks on its NeRF are estimated by our FLNeRF and fed to our modified MoFaNeRF to drive the right face's expression.

generated face NeRF to obtain accurate landmarks prediction. Finally, we use the predicted landmarks as input to the modified MoFaNeRF, together with texture map of another person, so that we obtain face NeRF of another person with our desired expression. Refer to the video in our GitHub where we can render face images from any viewpoint.

5. Experiments

5.1. Training and Testing

To balance training speed and sampling fidelity, the resolution of NeRF sampling box in the coarse model and fine model is $64 \times 64 \times 64$. The coarse model and fine model are trained separately. We select 100 identities from FaceScape dataset to perform data augmentation for coarse and fine models. Furthermore, 5 extra identities are chosen for testing with data augmentation. When training the fine model, to simulate predicted results of the coarse model, we add noise to the head location, orientation, and landmarks to make our fine model robust. Centers of the sampling boxes are shifted along x , y and z axis with a random number whose absolute value is smaller than 10 percent of the range the landmarks spanned along that axis. Random noises within $\pm 10^\circ$ are added to the rotation angles of sampling boxes.

When training the coarse and fine model, we set learning rate to 0.001 and batch size 32. The learning rate will finally decay to $8e-6$. We train our coarse model for 100 epochs and fine model for 50 epochs. We train our FLNeRF on 4x GTX 1080 GPUs. Training coarse model takes around 8 hours and fine model takes around 12 hours.

5.2. Ablation Study

5.2.1 3D landmarks detector on the NeRF

We show in Fig. 8 our qualitative results on 3D landmark detection from NeRFs. Table 1 tabulates the ablation on:



Figure 8. Accurate 3D landmarks detection of FLNeRF.

- (a) Remove fine model.
- (b) Remove TPS.
- (c) Use only two sampling scales, i.e., the first two rows in Fig. 2.
- (d) Our model without any modification.

We find that the accuracy of (c) and (d) are very close, where the accuracy of the results on some test subjects of (d) exceeds (c). However, the loss in (d) for eyes, which are the most expressive facial features, is always smaller than that of (c). We also notice that the variance of (d) is quite large compared with (c), which may be caused by introducing more parameters in extracting local features. We believe this is a bias-variance trade-off.

Table 1. As mentioned in Sec. 3.5.1, train/test data for coarse model only contain 20 discrete expressions. Here, we only calculate the average Wing loss on these expressions. For (b), (c) and (d), the All expression losses are calculated in the test data set with 110 different expressions. Mouth, Eyes, and Exaggerated Expressions loss measure the corresponding landmarks’ accuracy based on Wing loss. All the values in the table are multiplied by 10.

	All Expressions	Mouth	Eyes	Exaggerated Expression
(a)	2.55 ± 0.94	-	-	-
(b)	1.19 ± 0.31	1.25 ± 0.65	1.09 ± 0.19	1.70 ± 0.51
(c)	0.94 ± 0.17	0.96 ± 0.17	0.88 ± 0.07	0.91 ± 0.07
(d)	0.92 ± 0.21	0.94 ± 0.46	0.83 ± 0.09	0.90 ± 0.16

5.2.2 Our modified MoFaNeRF (2-code)

Ablation conducted on [93] and our modified version can be found in the appendix:

- (a) Original MoFaNeRF.
- (b) Using 3 codes: texture, shape and landmark.
- (c) (Our model) Using 2 codes: texture and landmark.

6. Concluding Remarks

Limitations. While FaceScape [88] is an excellent dataset, each image contains one head with clean background so extending FLNeRF for images captured in-the-wild is future work. Also, FaceScape does not model the inside of mouth (e.g., teeth), and landmarks around eyes are not accurately labeled. Thus our detection on closed eye is not as accurate, and inside of mouth in rendered images of our modified MoFaNeRF after applying refineNet may have artifacts.

Conclusion. We propose the first 3D coarse-to-fine face landmarks detector (FLNeRF) with multi-scale sampling that directly predicts accurate 3D landmarks on NeRF. Our FLNeRF is trained on augmented dataset with 110 discrete expressions generated by local and non-linear NeRF warp, which enables FLNeRF to give accurate landmarks prediction on a large number of complex expressions. We modify MoFaNeRF [93] as our application model. By connecting our application model and FLNeRF, we support various attractive downstream tasks such as face swapping and face

editing by directly operating predicted landmarks on face NeRFs. We hope FLNeRFs can enable future works on more accurate and generalized 3D face landmarks detection on NeRF and higher quality 3D face landmarks dataset.

References

- [1] Locating facial features with an extended active shape model. In David A. Forsyth, Philip H. S. Torr, and Andrew Zisserman, editors, *European Conference on Computer Vision (ECCV)*, 2008. 2
- [2] ShahRukh Athar, Zexiang Xu, Kalyan Sunkavalli, Eli Shechtman, and Zhixin Shu. Rignerf: Fully controllable neural 3d portraits. In *IEEE/CVF Conference on Computer Vision and Pattern Recognition (CVPR)*, 2022. 2, 3
- [3] Parama Bagchi, Debotosh Bhattacharjee, and Mita Nasipuri. Reg3dfacedptd: Registration of 3d point clouds using a common set of landmarks for alignment of human face images. *Künstliche Intell.*, 33(4):369–387, 2019. 3
- [4] Volker Blanz and Thomas Vetter. A morphable model for the synthesis of 3d faces. In *Proceedings of the 26th Annual Conference on Computer Graphics and Interactive Techniques, SIGGRAPH*, pages 187–194, 1999. 2
- [5] F.L. Bookstein. Principal warps: thin-plate splines and the decomposition of deformations. *IEEE Transactions on Pattern Analysis and Machine Intelligence*, 11(6):567–585, 1989. 5
- [6] Hao Chen, Qi Dou, Lequan Yu, and Pheng-Ann Heng. Voxresnet: Deep voxelwise residual networks for volumetric brain segmentation. *arXiv preprint arXiv:1608.05895*, 2016. 4
- [7] Hsiao-yu Chen, Edith Tretschk, Tuur Stuyck, Petr Kadlec, Ladislav Kavan, Etienne Vouga, and Christoph Lassner. Virtual elastic objects. In *IEEE/CVF Conference on Computer Vision and Pattern Recognition (CVPR)*, pages 15827–15837, June 2022. 2
- [8] Forrester Cole, Kyle Genova, Avneesh Sud, Daniel Vlasic, and Zhoutong Zhang. Differentiable surface rendering via non-differentiable sampling. In *IEEE/CVF International Conference on Computer Vision (ICCV)*, 2021. 2
- [9] Timothy F. Cootes, Gareth J. Edwards, and Christopher J. Taylor. Active appearance models. In Hans Burkhardt and Bernd Neumann, editors, *European Conference on Computer Vision (ECCV)*, pages 484–498, 1998. 2
- [10] Timothy F. Cootes and Christopher J. Taylor. Active shape models - ‘smart snakes’. In David C. Hogg and Roger Boyle, editors, *British Machine Vision Conference (BMVC)*, 1992. 2
- [11] Timothy F. Cootes, Christopher J. Taylor, David H. Cooper, and Jim Graham. Active shape models-their training and application. *Comput. Vis. Image Underst.*, 61(1):38–59, 1995. 2
- [12] Clement Creusot, Nick E. Pears, and Jim Austin. A machine-learning approach to keypoint detection and landmarking on 3d meshes. *Int. J. Comput. Vis.*, 102(1-3):146–179, 2013. 3
- [13] João Otávio de Lucena, João Paulo Lima, Diego Thomas, and Veronica Teichrieb. Real-time facial motion capture using rgb-d images under complex motion and occlusions. In *2019 21st Symposium on Virtual and Augmented Reality (SVR)*, pages 120–129, 2019. 3
- [14] Yu Deng, Jiaolong Yang, Jianfeng Xiang, and Xin Tong. Gram: Generative radiance manifolds for 3d-aware image generation. In *IEEE/CVF Conference on Computer Vision and Pattern Recognition (CVPR)*, 2022. 2, 3
- [15] Yilun Du, Yanan Zhang, Hong-Xing Yu, Joshua B. Tenenbaum, and Jiajun Wu. Neural radiance flow for 4d view synthesis and video processing. In *IEEE/CVF International Conference on Computer Vision (ICCV)*, 2021. 2
- [16] Xin Fan, Qi Jia, Kang Huyan, Xianfeng Gu, and Zhongxuan Luo. 3d facial landmark localization using texture regression via conformal mapping. *Pattern Recognit. Lett.*, 83:395–402, 2016. 3
- [17] Yao Feng, Fan Wu, Xiaohu Shao, Yanfeng Wang, and Xi Zhou. Joint 3d face reconstruction and dense alignment with position map regression network. In *European Conference on Computer Vision (ECCV)*, pages 557–574, 2018. 2
- [18] Zhen-Hua Feng, Josef Kittler, Muhammad Awais, Patrik Huber, and Xiao-Jun Wu. Wing loss for robust facial landmark localisation with convolutional neural networks. In *Proceedings of the IEEE Conference on Computer Vision and Pattern Recognition (CVPR)*, June 2018. 4
- [19] Guy Gafni, Justus Thies, Michael Zollhöfer, and Matthias Nießner. Dynamic neural radiance fields for monocular 4d facial avatar reconstruction. In *IEEE/CVF Conference on Computer Vision and Pattern Recognition (CVPR)*, pages 8649–8658, June 2021. 2, 3
- [20] Chen Gao, Yichang Shih, Wei-Sheng Lai, Chia-Kai Liang, and Jia-Bin Huang. Portrait neural radiance fields from a single image. *arXiv preprint arXiv:2012.05903*, 2020. 3
- [21] Stephan J. Garbin, Marek Kowalski, Matthew Johnson, Jamie Shotton, and Julien Valentin. Fastnerf: High-fidelity neural rendering at 200fps. In *IEEE/CVF International Conference on Computer Vision (ICCV)*, 2021. 2
- [22] Jianzhu Guo, Xiangyu Zhu, Yang Yang, Fan Yang, Zhen Lei, and Stan Z. Li. Towards fast, accurate and stable 3d dense face alignment. In Andrea Vedaldi, Horst Bischof, Thomas Brox, and Jan-Michael Frahm, editors, *European Conference on Computer Vision (ECCV)*, pages 152–168, 2020. 2
- [23] Longteng Guo, Danni Ai, Hong Song, and Jian Yang. Multi-scale landmark localization network for 3d facial point clouds. In *ICDSP 2021: 5th International Conference on Digital Signal Processing*, pages 86–93, 2021. 3
- [24] Michelle Guo, Alireza Fathi, Jiajun Wu, and Thomas Funkhouser. Object-centric neural scene rendering. *arXiv preprint arXiv:2012.08503*, 2020. 2
- [25] Peter Hedman, Pratul P. Srinivasan, Ben Mildenhall, Jonathan T. Barron, and Paul Debevec. Baking neural radiance fields for real-time view synthesis. In *IEEE/CVF International Conference on Computer Vision (ICCV)*, 2021. 2
- [26] Yang Hong, Bo Peng, Haiyao Xiao, Ligang Liu, and Juyong Zhang. Headnerf: A real-time nerf-based parametric head model. In *IEEE/CVF Conference on Computer Vision and Pattern Recognition (CVPR)*, 2022. 2, 3
- [27] Tao Hu, Shu Liu, Yilun Chen, Tiancheng Shen, and Jiaya Jia. Efficientnerf: Efficient neural radiance fields. In *IEEE/CVF Conference on Computer Vision and Pattern Recognition (CVPR)*, 2022. 2

- [28] Yuheng Jiang, Suyi Jiang, Guoxing Sun, Zhuo Su, Kaiwen Guo, Minye Wu, Jingyi Yu, and Lan Xu. Neurfusion: Neural volumetric rendering under human-object interactions. *arXiv preprint arXiv:2202.12825*, 2022. 2
- [29] M. M. Johari, Y. Lepoittevin, and F. Fleuret. Geonerf: Generalizing nerf with geometry priors. In *IEEE/CVF Conference on Computer Vision and Pattern Recognition (CVPR)*, 2022. 2
- [30] Abhijit Kundu, Kyle Genova, Xiaoqi Yin, Alireza Fathi, Caroline Pantofaru, Leonidas Guibas, Andrea Tagliasacchi, Frank Dellaert, and Thomas Funkhouser. Panoptic Neural Fields: A Semantic Object-Aware Neural Scene Representation. In *IEEE/CVF Conference on Computer Vision and Pattern Recognition (CVPR)*, 2022. 2
- [31] Weijian Li, Yuhang Lu, Kang Zheng, Haofu Liao, Chihung Lin, Jiebo Luo, Chi-Tung Cheng, Jing Xiao, Le Lu, Chang-Fu Kuo, and Shun Miao. Structured landmark detection via topology-adapting deep graph learning. In *European Conference on Computer Vision (ECCV)*, pages 266–283, 2020. 2
- [32] Zhengqi Li, Simon Niklaus, Noah Snavely, and Oliver Wang. Neural scene flow fields for space-time view synthesis of dynamic scenes. In *IEEE/CVF Conference on Computer Vision and Pattern Recognition (CVPR)*, 2020. 2
- [33] David B. Lindell, Julien N.P. Martel, and Gordon Wetzstein. AutoInt: Automatic integration for fast neural volume rendering. In *IEEE/CVF Conference on Computer Vision and Pattern Recognition (CVPR)*, 2021. 2
- [34] Lingjie Liu, Jiatao Gu, Kyaw Zaw Lin, Tat-Seng Chua, and Christian Theobalt. Neural sparse voxel fields. In *Advances in Neural Information Processing Systems (NeurIPS)*, 2020. 2
- [35] Rosanne Liu, Joel Lehman, Piero Molino, Felipe Petroski Such, Eric Frank, Alex Sergeev, and Jason Yosinski. An intriguing failing of convolutional neural networks and the coordconv solution. In *Advances in Neural Information Processing Systems (NeurIPS)*, 2018. 4
- [36] Steven Liu, Xiuming Zhang, Zhoutong Zhang, Richard Zhang, Jun-Yan Zhu, and Bryan Russell. Editing conditional radiance fields. In *IEEE/CVF International Conference on Computer Vision (ICCV)*, 2021. 2
- [37] Jiang-Jing Lv, Xiaohu Shao, Junliang Xing, Cheng Cheng, and Xi Zhou. A deep regression architecture with two-stage re-initialization for high performance facial landmark detection. In *IEEE/CVF Conference on Computer Vision and Pattern Recognition (CVPR)*, pages 3691–3700, 2017. 2
- [38] Ben Mildenhall, Pratul P. Srinivasan, Matthew Tancik, Jonathan T. Barron, Ravi Ramamoorthi, and Ren Ng. Nerf: Representing scenes as neural radiance fields for view synthesis. In *European Conference on Computer Vision (ECCV)*, 2020. 1, 4
- [39] Ben Mildenhall, Pratul P. Srinivasan, Matthew Tancik, Jonathan T. Barron, Ravi Ramamoorthi, and Ren Ng. Nerf: Representing scenes as neural radiance fields for view synthesis. In *European Conference on Computer Vision (ECCV)*, 2020. 2
- [40] Norman Müller, Andrea Simonelli, Lorenzo Porzi, Samuel Rota Bulò, Matthias Nießner, and Peter Kotschieder. Autorf: Learning 3d object radiance fields from single view observations. In *IEEE/CVF Conference on Computer Vision and Pattern Recognition (CVPR)*, 2022. 2
- [41] Prathap M. Nair and Andrea Cavallaro. 3-d face detection, landmark localization, and registration using a point distribution model. *IEEE Trans. Multimed.*, 11(4):611–623, 2009. 2
- [42] Michael Niemeyer and Andreas Geiger. Giraffe: Representing scenes as compositional generative neural feature fields. In *IEEE/CVF Conference on Computer Vision and Pattern Recognition (CVPR)*, 2020. 2
- [43] Atsuhiko Noguchi, Xiao Sun, Stephen Lin, and Tatsuya Harada. Neural articulated radiance field. In *IEEE/CVF International Conference on Computer Vision (ICCV)*, 2021. 2
- [44] Roy Or-El, Xuan Luo, Mengyi Shan, Eli Shechtman, Jeong Joon Park, and Ira Kemelmacher-Shlizerman. StyleSDF: High-Resolution 3D-Consistent Image and Geometry Generation. In *IEEE/CVF Conference on Computer Vision and Pattern Recognition (CVPR)*, pages 13503–13513, June 2022. 2, 3
- [45] Julian Ost, Fahim Mannan, Nils Thuerey, Julian Knodt, and Felix Heide. Neural scene graphs for dynamic scenes. In *IEEE/CVF Conference on Computer Vision and Pattern Recognition (CVPR)*, 2020. 2
- [46] Keunhong Park, Utkarsh Sinha, Jonathan T. Barron, Sofien Bouaziz, Dan B Goldman, Steven M. Seitz, and Ricardo Martin-Brualla. Nerfies: Deformable neural radiance fields. *IEEE/CVF International Conference on Computer Vision (ICCV)*, 2021. 2
- [47] Rasmus R. Paulsen, Kristine Aavild Juhl, Thilde Marie Haspang, Thomas F. Hansen, Melanie Ganz, and Gudmundur Einarsson. Multi-view consensus CNN for 3d facial landmark placement. *CoRR*, abs/1910.06007, 2019. 3
- [48] Sida Peng, Junting Dong, Qianqian Wang, Shangzhan Zhang, Qing Shuai, Xiaowei Zhou, and Hujun Bao. Animatable neural radiance fields for modeling dynamic human bodies. In *IEEE/CVF International Conference on Computer Vision (ICCV)*, 2021. 2
- [49] Albert Pumarola, Enric Corona, Gerard Pons-Moll, and Francesc Moreno-Noguer. D-nerf: Neural radiance fields for dynamic scenes. In *IEEE/CVF Conference on Computer Vision and Pattern Recognition (CVPR)*, 2020. 2
- [50] Marcos Quintana, Sezer Karaoglu, Federico Alvarez, José Manuel Menéndez, and Theo Gevers. Three-d wide faces (3DWF): facial landmark detection and 3d reconstruction over a new RGB-D multi-camera dataset. *Sensors*, 19(5):1103, 2019. 3
- [51] Daniel Rebain, Wei Jiang, Soroosh Yazdani, Ke Li, Kwang Moo Yi, and Andrea Tagliasacchi. Derf: Decomposed radiance fields. In *IEEE/CVF Conference on Computer Vision and Pattern Recognition (CVPR)*, 2020. 2
- [52] Christian Reiser, Songyou Peng, Yiyi Liao, and Andreas Geiger. Kilonerf: Speeding up neural radiance fields with thousands of tiny mlps. In *IEEE/CVF International Conference on Computer Vision (ICCV)*, 2021. 2
- [53] Sara Fridovich-Keil and Alex Yu, Matthew Tancik, Qinhong Chen, Benjamin Recht, and Angjoo Kanazawa. Plenoxels: Radiance fields without neural networks. In *IEEE/CVF*

Conference on Computer Vision and Pattern Recognition (CVPR), 2022. 2

- [54] Patrick Sauer, Timothy F. Cootes, and Christopher J. Taylor. Accurate regression procedures for active appearance models. In Jesse Hoey, Stephen J. McKenna, and Emanuele Trucco, editors, *British Machine Vision Conference, BMVC 2011, Dundee, UK, August 29 - September 2, 2011. Proceedings*, pages 1–11. BMVA Press, 2011. 2
- [55] Ruizhi Shao, Hongwen Zhang, He Zhang, Mingjia Chen, Yanpei Cao, Tao Yu, and Yebin Liu. Doublefield: Bridging the neural surface and radiance fields for high-fidelity human reconstruction and rendering. In *IEEE/CVF Conference on Computer Vision and Pattern Recognition (CVPR)*, 2022. 2
- [56] Sahil Sharma and Vijay Kumar. Voxel-based 3d occlusion-invariant face recognition using game theory and simulated annealing. *Multim. Tools Appl.*, 79(35-36):26517–26547, 2020. 2
- [57] Sahil Sharma and Vijay Kumar. 3d landmark-based face restoration for recognition using variational autoencoder and triplet loss. *IET Biom.*, 10(1):87–98, 2021. 2
- [58] Karen Simonyan and Andrew Zisserman. Very deep convolutional networks for large-scale image recognition. In Yoshua Bengio and Yann LeCun, editors, *3rd International Conference on Learning Representations, ICLR 2015, San Diego, CA, USA, May 7-9, 2015, Conference Track Proceedings*, 2015. 4
- [59] Mingli Song, Dacheng Tao, Shengpeng Sun, Chun Chen, and Stephen J. Maybank. Robust 3d face landmark localization based on local coordinate coding. *IEEE Trans. Image Process.*, 23(12):5108–5122, 2014. 2
- [60] Jinzhan Su, Zhe Wang, Chunyuan Liao, and Haibin Ling. Efficient and accurate face alignment by global regression and cascaded local refinement. In *IEEE Conference on Computer Vision and Pattern Recognition Workshops, CVPR Workshops 2019, Long Beach, CA, USA, June 16-20, 2019*, pages 267–276. Computer Vision Foundation / IEEE, 2019. 2
- [61] Mohammed Suhail, Carlos Esteves, Leonid Sigal, and Ameesh Makadia. Light field neural rendering. In *IEEE/CVF Conference on Computer Vision and Pattern Recognition (CVPR)*, 2022. 2
- [62] Federico M. Sukno, John L. Waddington, and Paul F. Whelan. 3-d facial landmark localization with asymmetry patterns and shape regression from incomplete local features. *IEEE Trans. Cybern.*, 45(9):1717–1730, 2015. 3
- [63] Cheng Sun, Min Sun, and Hwann-Tzong Chen. Direct voxel grid optimization: Super-fast convergence for radiance fields reconstruction. In *IEEE/CVF Conference on Computer Vision and Pattern Recognition (CVPR)*, 2022. 2
- [64] Jingxiang Sun, Xuan Wang, Yong Zhang, Xiaoyu Li, Qi Zhang, Yebin Liu, and Jue Wang. Fenerf: Face editing in neural radiance fields. *arXiv preprint arXiv:2111.15490*, 2021. 2, 3
- [65] Ke Sun, Bin Xiao, Dong Liu, and Jingdong Wang. Deep high-resolution representation learning for human pose estimation. *CoRR*, abs/1902.09212, 2019. 2
- [66] Yi Sun, Xiaogang Wang, and Xiaoou Tang. Deep convolutional network cascade for facial point detection. In *IEEE/CVF Conference on Computer Vision and Pattern Recognition (CVPR)*, pages 3476–3483. IEEE Computer Society, 2013. 2
- [67] Matthew Tancik, Ben Mildenhall, Terrance Wang, Divi Schmidt, Pratul P. Srinivasan, Jonathan T. Barron, and Ren Ng. Learned initializations for optimizing coordinate-based neural representations. In *IEEE/CVF Conference on Computer Vision and Pattern Recognition (CVPR)*, 2020. 2
- [68] Luan Tran and Xiaoming Liu. Nonlinear 3d face morphable model. In *IEEE/CVF Conference on Computer Vision and Pattern Recognition (CVPR)*, June 2018. 2
- [69] George Trigeorgis, Patrick Snape, Mihalios A. Nicolaou, Epameinondas Antonakos, and Stefanos Zafeiriou. Mnemonic descent method: A recurrent process applied for end-to-end face alignment. In *IEEE/CVF Conference on Computer Vision and Pattern Recognition (CVPR)*, pages 4177–4187, 2016. 2
- [70] George Trigeorgis, Patrick Snape, Mihalios A. Nicolaou, Epameinondas Antonakos, and Stefanos Zafeiriou. Mnemonic descent method: A recurrent process applied for end-to-end face alignment. In *IEEE/CVF Conference on Computer Vision and Pattern Recognition (CVPR)*, pages 4177–4187. IEEE Computer Society, 2016. 2
- [71] Roberto Valle, José Miguel Buenaposada, Antonio Valdés, and Luis Baumela. A deeply-initialized coarse-to-fine ensemble of regression trees for face alignment. In *European Conference on Computer Vision (ECCV)*, 2018. 2
- [72] Liao Wang, Jiakai Zhang, Xinhang Liu, Fuqiang Zhao, Yanshun Zhang, Yingliang Zhang, Minye Wu, Jingyi Yu, and Lan Xu. Fourier plenotrees for dynamic radiance field rendering in real-time. In *IEEE/CVF Conference on Computer Vision and Pattern Recognition (CVPR)*, pages 13524–13534, June 2022. 2
- [73] Chung-Yi Weng, Brian Curless, Pratul P. Srinivasan, Jonathan T. Barron, and Ira Kemelmacher-Shlizerman. HumanNeRF: Free-viewpoint rendering of moving people from monocular video. In *IEEE/CVF Conference on Computer Vision and Pattern Recognition (CVPR)*, pages 16210–16220, June 2022. 2
- [74] Cho-Ying Wu, Qiangeng Xu, and Ulrich Neumann. Synergy between 3dmm and 3d landmarks for accurate 3d facial geometry. In *International Conference on 3D Vision (3DV)*, 2021. 2, 4
- [75] Wayne Wu, Chen Qian, Shuo Yang, Quan Wang, Yici Cai, and Qiang Zhou. Look at boundary: A boundary-aware face alignment algorithm. *CoRR*, abs/1805.10483, 2018. 2
- [76] Wenqi Xian, Jia-Bin Huang, Johannes Kopf, and Changil Kim. Space-time neural irradiance fields for free-viewpoint video. In *IEEE/CVF Conference on Computer Vision and Pattern Recognition (CVPR)*, 2020. 2
- [77] Qiangeng Xu, Zexiang Xu, Julien Philip, Sai Bi, Zhixin Shu, Kalyan Sunkavalli, and Ulrich Neumann. Pointnerf: Point-based neural radiance fields. *arXiv preprint arXiv:2201.08845*, 2022. 2
- [78] Tianhan Xu, Yasuhiro Fujita, and Eiichi Matsumoto. Surface-aligned neural radiance fields for controllable 3d human synthesis. In *IEEE/CVF Conference on Computer Vision and Pattern Recognition (CVPR)*, 2022. 2
- [79] Bangbang Yang, Yinda Zhang, Yinghao Xu, Yijin Li, Han Zhou, Hujun Bao, Guofeng Zhang, and Zhaopeng Cui. Learning object-compositional neural radiance field for editable scene rendering. In *IEEE/CVF International Conference on Computer Vision (ICCV)*, October 2021. 2

- [80] Gengshan Yang, Minh Vo, Neverova Natalia, Deva Ramanan, Vedaldi Andrea, and Joo Hanbyul. Banmo: Building animatable 3d neural models from many casual videos. In *IEEE/CVF Conference on Computer Vision and Pattern Recognition (CVPR)*, 2022. [2](#)
- [81] Alex Yu, Ruilong Li, Matthew Tancik, Hao Li, Ren Ng, and Angjoo Kanazawa. PlenOctrees for real-time rendering of neural radiance fields. In *IEEE/CVF International Conference on Computer Vision (ICCV)*, 2021. [2](#)
- [82] Wentao Yuan, Zhaoyang Lv, Tanner Schmidt, and Steven Lovegrove. Star: Self-supervised tracking and reconstruction of rigid objects in motion with neural rendering. In *IEEE/CVF Conference on Computer Vision and Pattern Recognition (CVPR)*, pages 13144–13152, 2021. [2](#)
- [83] Hongwen Zhang, Qi Li, and Zhenan Sun. Joint voxel and coordinate regression for accurate 3d facial landmark localization. In *24th International Conference on Pattern Recognition, ICPR 2018, Beijing, China, August 20-24, 2018*, pages 2202–2208. IEEE Computer Society, 2018. [2](#)
- [84] Kai Zhang, Gernot Riegler, Noah Snaveley, and Vladlen Koltun. Nerf++: Analyzing and improving neural radiance fields. *arXiv:2010.07492*, 2020. [2](#)
- [85] Zhanpeng Zhang, Wei Zhang, Jianzhuang Liu, and Xiaoou Tang. Multiview facial landmark localization in RGB-D images via hierarchical regression with binary patterns. *IEEE Trans. Circuits Syst. Video Technol.*, 24(9):1475–1485, 2014. [3](#)
- [86] Fuqiang Zhao, Wei Yang, Jiakai Zhang, Pei Lin, Yingliang Zhang, Jingyi Yu, and Lan Xu. Humannerf: Efficiently generated human radiance field from sparse inputs. In *IEEE/CVF Conference on Computer Vision and Pattern Recognition (CVPR)*, pages 7743–7753, June 2022. [2](#)
- [87] Zerong Zheng, Han Huang, Tao Yu, Hongwen Zhang, Yandong Guo, and Yebin Liu. Structured local radiance fields for human avatar modeling. In *IEEE/CVF Conference on Computer Vision and Pattern Recognition (CVPR)*, June 2022. [2](#)
- [88] Hao Zhu, Haotian Yang, Longwei Guo, Yidi Zhang, Yanru Wang, Mingkai Huang, Qiu Shen, Ruigang Yang, and Xun Cao. Facescape: 3d facial dataset and benchmark for single-view 3d face reconstruction. *arXiv preprint arXiv:2111.01082*, 2021. [2](#), [4](#), [5](#), [8](#), [13](#), [14](#)
- [89] Meilu Zhu, Daming Shi, Mingjie Zheng, and Muhammad Sadiq. Robust facial landmark detection via occlusion-adaptive deep networks. In *IEEE/CVF Conference on Computer Vision and Pattern Recognition (CVPR)*, pages 3481–3491, 2019. [2](#)
- [90] Shizhan Zhu, Cheng Li, Chen Change Loy, and Xiaoou Tang. Face alignment by coarse-to-fine shape searching. In *IEEE/CVF Conference on Computer Vision and Pattern Recognition (CVPR)*, pages 4998–5006. IEEE Computer Society, 2015. [2](#)
- [91] Xiangyu Zhu, Zhen Lei, Xiaoming Liu, Hailin Shi, and Stan Z. Li. Face alignment across large poses: A 3d solution. In *IEEE/CVF Conference on Computer Vision and Pattern Recognition (CVPR)*, pages 146–155. IEEE Computer Society, 2016. [2](#)
- [92] Xiangyu Zhu, Chang Yu, Di Huang, Zhen Lei, Hao Wang, and Stan Z. Li. Beyond 3dmm: Learning to capture high-fidelity 3d face shape. *CoRR*, abs/2204.04379, 2022. [3](#)
- [93] Yiyu Zhuang, Hao Zhu, Xusen Sun, and Xun Cao. Mofanerf: Morphable facial neural radiance field. In *European Conference on Computer Vision (ECCV)*, 2022. [2](#), [3](#), [6](#), [7](#), [8](#), [13](#)

A. TPS

The coefficients \mathbf{A}_0 , \mathbf{A}_1 and ω_i mentioned in section 3.5.2 can be found by solving the following linear system. Let $\mathbf{W} = [\omega_1, \dots, \omega_N]$ and $\mathbf{Y} = [\mathbf{L}'^\top \mathbf{0} \mathbf{0} \mathbf{0} \mathbf{0}]^\top$:

$$\mathbf{K} = \begin{bmatrix} 0 & U(\|\mathbf{l}_1 - \mathbf{l}_2\|) & \dots & U(\|\mathbf{l}_1 - \mathbf{l}_N\|) \\ U(\|\mathbf{l}_2 - \mathbf{l}_1\|) & 0 & \dots & U(\|\mathbf{l}_2 - \mathbf{l}_N\|) \\ \dots & \dots & \dots & \dots \\ U(\|\mathbf{l}_N - \mathbf{l}_1\|) & U(\|\mathbf{l}_N - \mathbf{l}_2\|) & \dots & 0 \end{bmatrix}_{N \times N} \quad (7)$$

$$\mathbf{P} = \begin{bmatrix} \mathbf{1} & \mathbf{l}_1^\top \\ \mathbf{1} & \mathbf{l}_2^\top \\ \dots & \dots \\ \mathbf{1} & \mathbf{l}_n^\top \end{bmatrix}_{N \times 4} \quad (8)$$

$$\mathbf{M} = \begin{bmatrix} \mathbf{K} & \mathbf{P} \\ \mathbf{P}^\top & \mathbf{0} \end{bmatrix}_{(N+4) \times (N+4)} \quad (9)$$

$$(\mathbf{W} | \mathbf{A}_1 \mathbf{A}_0)^\top = \mathbf{M}^{-1} \mathbf{Y} \quad (10)$$

B. Ablation study

B.1. 3D landmarks detector on the NeRF

Table 2 tabulates the ablation on (using VGG backbone):

- (a) Remove fine model.
- (b) Remove TPS.
- (c) Use only two sampling scales, i.e., the first two rows in Figure 2.
- (d) Our model without any modification.

We follow the same test strategy as section 5.2.1 to conduct this experiment. Similar to the results obtained by VoxResNet backbone, FLNeRF achieves the best among all ablation studies using VGG backbone. And the bias-variance trade-off can also be observed here.

Table 2. The table is calculated in the same way as the Table 1. in the main paper except the backbone. All the values in the table are multiplied by 10.

	All Expressions	Mouth	Eyes	Exaggerated Expression
(a)	2.49±0.91	-	-	-
(b)	0.94±0.22	0.97±0.52	0.86±0.090	1.27±0.44
(c)	0.90±0.069	0.88±0.37	0.88±0.048	0.86±0.048
(d)	0.86±0.084	0.87±0.39	0.85±0.062	0.84±0.076

B.2. Our modified MoFaNeRF (2-code)

- (a) Original MoFaNeRF.
- (b) Using 3 codes: texture, shape and landmark.
- (c) (Our model) Using 2 codes: texture and landmark.

We render 300 images of the first 15 identities in our dataset [88] for evaluation, where one image is synthesized for every expression and every identity with random view

direction. Following [93], we use PSNR, SSIM and LPIPS criteria to assess objective, structural, and perceptual similarity, respectively. Tab. 3 tabulates the quantitative statistics on the corresponding coarse models.

Table 3. Quantitative evaluation of on our application model. (a) is original MoFaNeRF, (b) is our 3-code (texture, shape, landmark) MoFaNeRF model, (c) is our 2-code (texture, landmark) MoFaNeRF model. With our landmarks which effectively encode 3D shape, the original shape code in MoFaNeRF can be eliminated while outperforming (a) and (b). Values of SSIM and LPIPS are multiplied by 10.

	PSNR(dB)↑	SSIM↑	LPIPS↓	# params
(a)	24.85±1.91	8.53±0.35	1.72±0.32	29,100,936
(b)	21.71±1.46	7.28±0.50	3.50±0.42	29,584,776
(c)	25.47±1.68	8.60±0.32	1.66±0.28	29,456,776

From the testing statistics, our model outperforms (a) and (b). Interestingly, comparing (b) and (c), adding shape code as input substantially decreases performance, indicating the shape code does have redundant information with 3D landmarks. For a given identity with different expressions, the shape code remains the same while landmarks vary which confuses the network in (b). Comparing (a) with (c), raw 3D landmarks location outperforms combination of shape and learnable expression code. We believe that (a) attempts to extract deep information from each expression that is independent from the shape code, where such information mainly comes from 3D landmarks.

Figure 6 in our main paper presents the qualitative results, showing that we can independently control movements of mouth, nose, eyes, and eyebrows by directly manipulating landmarks owing to our better disentanglement than [93] in their shape and expression codes, and our better objective, structural, and perceptual similarity as validated in Tab. 3.

C. More Visualization Results

C.1. 3D landmarks detection on the NeRF

As extension of Figure 8 in our main paper, Fig. 9 shows more visualization results of accurate 3D landmarks prediction of our FLNeRF on face NeRFs. Observing the two figures, we can see how robust our FLNeRF is, that it predicts accurate 3D face landmarks for both males and females, people with various skin colors, faces under different illuminations, and even faces with glasses and beard.

C.2. Video

Please watch the demo video in our Github website.

By capitalizing our accurate 3D face landmarks, our modified MoFaNeRF could perform various downstream tasks, like face swapping and face editing introduced in section 4 in our main paper. Here we produce a video for more direct visualization. The video contains four parts:



Figure 9. More visualization of accurate 3D landmarks detection of FLNeRF.

1. **Accurate 3D face landmarks detection on NeRF.** Each row shows the visualization of the accurate 3D facial landmarks detection on the same identity from 3 different camera poses. The landmarks overlapped on the face NeRF are the estimated facial landmarks.
2. **Face editing by directly manipulating 3D face landmarks.** The two columns show the results obtained by manipulating 3D face landmarks on two different identities using our modified MoFaNeRF. The results are coherent in expression transitions and consistent in different view directions. The landmarks overlapped on the face NeRF are the target landmarks.
3. **3D face reenactment on NeRF.** For 3D face reenactment, we use FLNeRF to predict 3D face landmarks, given any face NeRF. The left face in the video is driver face NeRF with estimated landmarks overlaid. The predicted landmarks are fed together with the same person’s texture map to our modified MoFaNeRF, which then produce the right face in the video.
4. **3D expression transfer on NeRF.** For 3D expression transfer, we use FLNeRF to predict 3D face landmarks on \mathcal{I}_1 ’s face NeRF. The left face in the video is driver face NeRF (\mathcal{I}_1 ’s face NeRF) with estimated landmarks overlaid. The predicted landmarks are fed together with \mathcal{I}_2 ’s texture map to our modified MoFaNeRF, which then produce the right face in the video (\mathcal{I}_2 ’s face NeRF).

This video demonstrates that our FLNeRF could produce accurate 3D face landmarks on NeRF. Furthermore, with the help of our modified MoFaNeRF, FLNeRF could directly operate on dynamic NeRF, so an animator can easily edit, control, and even transfer emotion from another face NeRF.

D. Ethics Discussions

Images we use for training, testing and visualization in this paper are from FaceScape [88], an open dataset. The images are used only for research purpose. Our technology has the potential to cheat face recognition system. Therefore, it should be abused for illegal purposes.